Environmental Science & Technology

Subscriber access provided by Duquesne University - Gumberg Library

Remediation and Control Technologies

Formation and aggregation of lead phosphate particles: Implications for lead immobilization in water supply systems

Juntao Zhao, Daniel E. Giammar, Jill D. Pasteris, Chong Dai, Yeunook Bae, and Yandi Hu

Environ. Sci. Technol., **Just Accepted Manuscript** • DOI: 10.1021/acs.est.8b02788 • Publication Date (Web): 25 Sep 2018

Downloaded from http://pubs.acs.org on September 26, 2018

Just Accepted

"Just Accepted" manuscripts have been peer-reviewed and accepted for publication. They are posted online prior to technical editing, formatting for publication and author proofing. The American Chemical Society provides "Just Accepted" as a service to the research community to expedite the dissemination of scientific material as soon as possible after acceptance. "Just Accepted" manuscripts appear in full in PDF format accompanied by an HTML abstract. "Just Accepted" manuscripts have been fully peer reviewed, but should not be considered the official version of record. They are citable by the Digital Object Identifier (DOI®). "Just Accepted" is an optional service offered to authors. Therefore, the "Just Accepted" Web site may not include all articles that will be published in the journal. After a manuscript is technically edited and formatted, it will be removed from the "Just Accepted" Web site and published as an ASAP article. Note that technical editing may introduce minor changes to the manuscript text and/or graphics which could affect content, and all legal disclaimers and ethical guidelines that apply to the journal pertain. ACS cannot be held responsible for errors or consequences arising from the use of information contained in these "Just Accepted" manuscripts.

ACS Publications

is published by the American Chemical Society. 1155 Sixteenth Street N.W., Washington, DC 20036

Published by American Chemical Society. Copyright © American Chemical Society. However, no copyright claim is made to original U.S. Government works, or works produced by employees of any Commonwealth realm Crown government in the course of their duties.

Formation and aggregation of lead phosphate particles: Implications for lead immobilization in water supply systems

Juntao Zhao[1], Daniel E. Giammar[2], Jill D. Pasteris[3], Chong Dai[1], Yeunook Bae[2], and Yandi Hu[1]*

[1]*Department of Civil & Environmental Engineering,*

University of Houston, Houston, TX 77004

[2]*Department of Energy, Environmental and Chemical Engineering,*

Washington University in St. Louis, St. Louis, MO 63130

[3]*Department of Earth and Planetary Sciences,*

Washington University in St. Louis, St. Louis, MO 63130

***To Whom Correspondence Should Be Addressed**

E-mail: yhu11@uh.edu

Phone: (713)743-4285

Fax: (713)743-4260

http://www.cive.uh.edu/faculty/hu

Submitted: May 2018

Revised : September 2018

Environmental Science & Technology

Abstract

Phosphate is commonly added to drinking water to inhibit lead release from lead service lines and lead-containing materials in premise plumbing. Phosphate addition promotes the formation of lead phosphate particles, and their aggregation behavior may affect their transport in pipes. Here, lead phosphate formation and aggregation were studied under varied aqueous conditions typical of water supply systems. Under high aqueous PO_4/Pb molar ratios (> 1), phosphate adsorption made the particles more negatively charged. Therefore, enhanced stability of lead phosphate particles was observed, suggesting that although addition of excess phosphate can lower the dissolved lead concentrations in tap water, it may increase concentrations of particulate lead. Adsorption of divalent cations (Ca^{2+} and Mg^{2+}) onto lead phosphate particles neutralized their negative surface charges and promoted their aggregation at pH 7, indicating that phosphate addition for lead immobilization may be more efficient in harder waters. The presence of natural organic matter (NOM, ≥ 0.05 mg C/L humic acid and ≥ 0.5 mg C/L fulvic acid) retarded particle aggregation at pH 7. Consequently, removal of organic carbon during water treatment to lower the formation of disinfection-by-products (DBPs) may have the additional benefit of minimizing the mobility of lead-containing particles. This study provided insight into fundamental mechanisms controlling lead phosphate aggregation. Such understanding is helpful to understand the observed trends of total lead in water after phosphate addition in both field and pilot-scale lead pipe studies. Also, it can help optimize lead immobilization by better controlling the water chemistry during phosphate addition.

Introduction

Lead consumption can pose severe health risk to the public by impairing human nervous, digestive, hematopoietic, cardiovascular, and urinary systems.[1,2] Before 1986, lead pipes were used as service lines for water supply to connect buildings to water mains.[3] Lead can be released into drinking water from lead pipes and scales of lead-containing corrosion products on the pipes, lead-bearing brass, copper/lead solder joints, and galvanized iron pipes.[4–10] For lead corrosion control, an action level of 15 μg/L was set by the Lead and Copper Rule (LCR) for the total lead concentration in water systems serving more than 50,000 people .[11]

However, occurrences of elevated lead concentrations in tap water are common nation-wide mainly due to lead service lines (LSL) disturbance and water chemistry changes.[12–14] A variety of water chemistry parameters can affect lead release from pipes, including pH, alkalinity, temperature, and the presence of iron particulates and NOM.[15–24] Inadequate and inappropriate use of disinfectants and corrosion inhibitors can also lead to elevated lead concentrations in tap water.[25–27] From 2001 to 2004, due to the switch of water disinfectants, high lead concentrations were observed in Washington DC tap water.[27,28] During the recent water crisis in Flint, MI (started in April 2014), the lack of phosphate addition and switch of sulfate to chloride-based coagulants resulted in extensive iron and lead release.[29] Lead concentrations over hazardous waste level of 5,000 μg/L were detected in tap water.[30]

To control lead corrosion and release, water chemistry of the treated drinking water can be adjusted.[31–37] Dissolved lead concentrations can be controlled by the dissolution/precipitation of lead corrosion products (e.g., lead oxides, carbonates, and phosphates). Among various corrosion inhibitors (e.g., phosphate, silicate, etc.), phosphate is the

most widely used one to minimize lead corrosion in water supply systems.[38] In the absence of phosphates, cerussite ($PbCO_3$) and hydrocerussite ($Pb_3(CO_3)_2(OH)_2$) are common phases in pipe scale,[39] and dissolved lead concentrations in equilibrium with these phases can be higher than the action level (15 μg/L, 0.072 μM) of the Lead and Copper Rule. Phosphate addition can promote the precipitation of lead phosphate particles that are less soluble than lead carbonate phases and can provide equilibrium dissolved lead concentrations lower than 15 μg/L.[35,40–42]

When phosphate has been added to control lead release, total lead concentrations (dissolved + particulate lead) in tap water were reported to remain high (over 50 μg/L) for months after phosphate addition.[43–45] Pipe rig studies to evaluate the optimization of corrosion control treatment for the D.C. Water and Sewer Authority (DCWASA)'s distribution system indicated that it took six months of phosphate addition before lead concentrations consistently dropped below 15 μg/L.[44] Same observation was found in pipe systems of Providence, RI. After adding phosphoric acid for 5 months, high levels of total lead concentration occurred frequently, while dissolved lead concentrations decreased almost immediately and stayed low.[45] When the water crisis in Flint was reported, phosphate was added after its absence for 18 months. The total lead concentrations were reported to remain as high as 141 to 22, 905 μg/L at several residences for 6 months, which were 1-3 orders of magnitude higher than the action level (15 μg/L).[46] These reported high concentrations of total lead in tap water after phosphate addition indicated the possible transport of lead phosphate particles along the pipes to taps.

Pilot-scale studies have been conducted to investigate lead immobilization after phosphate addition under conditions relevant to water supply systems.[7,43,47] Churchill et al.

conducted a 12-month pilot plant study and found that the total lead concentrations at the pipe outlet were higher than 15 μg/L even after continuous phosphate addition for a half year.[43] Miller conducted pilot-scale experiments of orthophosphate addition with lead pipes, and it was reported that higher total lead removal efficiency was achieved with 1.0 mg PO_4/L instead of 5.0 mg PO_4/L addition.[47] Such observations showed that, although more phosphate addition can lower dissolved lead concentration, it might result in higher total lead concentration, suggesting the importance of transport of lead phosphate particles in pipes.

Effects of aqueous parameters (e.g., alkalinity and pH) on particulate lead stability in water supply systems have been studied without phosphate addition;[15,48] However, the formation and aggregation of lead phosphate particles under varied aqueous conditions relevant to drinking water supply systems have not been studied yet. Based on Derjaguin–Landau–Verwey–Overbeek (DLVO) theory and reported aggregation behaviors of other particles (e.g., magnetite, ferrihydrite and TiO_2), divalent cations generally promote particle aggregation by charge neutralization, while natural organic matter has been reported to retard or promote aggregation depending on solution conditions.[49–51] Ionic strength and pH also have great influence on aggregation behaviors of particles by affecting the thickness of the electric double layer and the surface protonation/deprotonation. [49–51]

This study aims to provide new information on factors governing the aggregation of freshly precipitated lead phosphate particles using dynamic light scattering (DLS). To mimic processes in pipe systems where lead phosphate formation and aggregation occur simultaneously, here lead and phosphate solutions were mixed to study the formation of lead phosphate nanoparticles and their subsequent aggregation. The effects of aqueous P/Pb ratios, ionic strength, and pH, as well as the presence of cations (Na^+, Ca^{2+}, and Mg^{2+}), anions (Cl^-, F^-,

and HCO_3^-), and natural organic matter (fulvic and humid acids) on lead phosphate aggregation were systematically investigated. To understand the controlling mechanisms, the morphology, compositions, phase, and zeta potentials of the particles were measured using scanning electron microscopy (SEM), inductively coupled plasma mass spectrometry (ICP-MS), Raman spectroscopy/grazing-incidence wide-angle X-ray scattering (GIWAXS), and DLS, respectively. The new insights provided here can optimize phosphate addition to control lead release and mobilization from lead pipes.

Experimental Section

Solution preparation

All solutions used in this study were prepared with ultrapure water (resistivity > 18 mΩ) equilibrated with atmospheric CO_2 (i.e., by purging with air overnight), except for the $NaHCO_3$ solution which was prepared using ultrapure water without aeration. Stock solutions of 1 mM $Pb(NO_3)_2$, 10 mM Na_2HPO_4, 10 mM NaH_2PO_4, 100 mM $NaNO_3$, 1.2 mM $Ca(NO_3)_2$, 1.2 mM $Mg(NO_3)_2$, 3.6 mM NaCl and 3.1 mM $NaHCO_3$ were prepared. Though the composition and properties of fresh-water NOM vary among different sites, the predominant species (from approximately 70 to > 90%) is reported to be humic substances (HS).[52] They are also considered as the most important components in relation to water treatment and corrosion processes.[53] Thus, fulvic acid and humic acid were used here as representatives of NOM, and their typical concentrations (0.1, 0.5, 2, and 5 mg C/L for fulvic acid and 0.05, 0.1, 0.5, 5 mg C/L for humic acid) in drinking water systems were chosen.[54,55] Stock solutions of fulvic acid (Suwannee River) and humic acid (Sigma Aldrich) were prepared, and the organic carbon contents were determined with a total organic carbon (TOC) analyzer (TOC-L, Shimadzu). Details of NOM sample preparation and TOC measurements can be found in the Supporting

Information. The stock solutions were then diluted to the desired concentrations (Table 1) using CO_2-equilibrated ultrapure water except for the $NaHCO_3$ solution.

Here, five sets of experiments were conducted (Table 1) to investigate the effects of total P/Pb ratios ($R_{P/Pb}$ = 1000, 100, 60, 10, and 1, set I), cations and anions (Na^+, Ca^{2+}, Mg^{2+}, NO_3^-, Cl^-, F^-, and HCO_3^-, set II), natural organic matter (fulvic acid with 0.1, 0.5, 2, and 5 mg C/L, and humic acid with 0.05, 0.1, 0.5, and 5 mg C/L, set III), ionic strength (IS = 0.58, 4, 11, 21, 30, 50, 80 and 99 mM, set IV), and pH (5.5, 7.0, and 8.5, set V) on lead phosphate formation and aggregation in solutions equilibrated with atmospheric CO_2 except for the experiment with $NaHCO_3$ solution. The mixtures of Na_2HPO_4 and NaH_2PO_4 solutions were used as the phosphate source and to adjust solutions' pH, and $NaNO_3$ was used to adjust solutions' ionic strength. Although ionic strength values greater than 11 mM are unlikely in drinking water, they were included in set IV to study the overall effects of ionic strength on the particle aggregation. For solutions with the addition of salts (sets II and IV) and NOM (set III), the Na_2HPO_4/NaH_2PO_4 solutions were first mixed with salt solution ($NaNO_3$, $Ca(NO_3)_2$, $Mg(NO_3)_2$, $CaCl_2$, NaCl, NaF, or $NaHCO_3$) or organic matter (fulvic or humic acid) and the mixed solution was vortexed for 5 s. Then $Pb(NO_3)_2$ solution was added to the mixed solution and lead phosphate precipitation started in the presence of salts or organics. To prepare a solution at pH 8.5 for experiment set V, Na_2HPO_4 was first mixed with NaOH, and then $Pb(NO_3)_2$ solution was added to the mixed solution. The effects of various concentrations (i.e., 0.1, 0.5, and 0.8 mM) of Ca^{2+} and Mg^{2+} on lead phosphate aggregation were also conducted, with detailed solution conditions in the Supporting Information (Table S3).

The solutions' pH, IS, and saturation index (SI) with respect to potential precipitates, i.e., $Pb_3(PO_4)_2$, $PbHPO_4$, pyromorphite-group minerals ($Pb_5(PO_4)_3OH$, $Pb_5(PO_4)_3Cl$, and

$Pb_5(PO_4)_3F$), cerussite, hydrocerussite, and lead hydroxide ($Pb(OH)_2$) were calculated using the Minteq database in Geochemist's Workbench (GWB, student version 11.0) (Table 1), with all solutions set to be in equilibrium with atmospheric CO_2 except for the $NaHCO_3$ solution. In pipes from real drinking water distribution systems after phosphate treatment, as well as in new pipes used in experiments after phosphate addition, Pb-orthophosphate minerals, such as chloropyromorphite and hydroxylpyromorphite, have been identified as corrosion scales.[56–58] In real drinking water systems, the initial total lead concentrations before treatment can be over the range of 50-5,000 μg/L,[30,56,57] and a great excess of phosphate (0.6-8.6 mg/L) relative to lead is added.[56,57] Here the initial SI with respect to hydroxylpyromorphite was estimated for a drinking water system equilibrated with air and having a solution pH of 7 and dissolved lead concentration of 100 μg/L, which is quite possible for a system that is out of compliance with the lead and copper rule (LCR). When a realistic dose of 3 mg/L phosphate is added for lead control, the initial SI with respect to hydroxylpyromorphite is calculated to be 10.7. To generate enough particles for accurate DLS measurements, here relatively higher lead and phosphate concentrations (Table 1) were used and the initial solutions' SI with respect to hydroxylpyromorphite ($Pb_5(PO_4)_3OH$) were similar (12.6 ± 0.1) in all solutions (Table 1). To separately investigate the effects of each water chemistry parameter ($R_{P/Pb}$, IS, cation/anion, NOM, or pH) for each set of experiments, solutions were prepared with fixed values for most of the other water chemistry parameters (Table 1).

Dynamic Light Scattering (DLS) Measurements

The formation and aggregation behaviors of particles formed in solution (Table 1, sets I-V) were explored by monitoring their size evolution in solutions by DLS (Zetasizer, Malvern Instrument Ltd.). Freshly prepared solution (Table 1) was shaken by hand for 5 s and then

injected into a 1-mL cuvette (ZEN0040, Malvern Instruments Ltd.). Size data were continuously collected every 15 s for 1 hr. In solutions with slow aggregation kinetics (i.e., no significant size changes within 1 hr), sizes of particles were also measured daily for 12 days to understand the long-term aggregation. To observe the morphology of particles in suspension, particles were collected from the precipitation/aggregation solutions (Table 1) by centrifuging at 5000 rpm for 1 minute, and the slurry was transferred to gold-coated silicon wafers. The wafers were then dried in a desiccator, and coated with gold before scanning electron microscopy (SEM, JEOL Ltd.) measurements. The detailed information about SEM measurements can be found in our previous publication and the Supporting Information..[59]

After the size measurement, the cuvette was equipped with a dip cell (ZEN1002, Malvern Instruments Ltd.) for electrophoretic mobility measurement of particles in all precipitation solutions (ξp, Table 1).[60–66] Zeta potential values (ξ) were calculated based on the following relationship with the measured electrophoretic mobility (U_E):

$$U_E = \frac{2\varepsilon\xi f(\kappa a)}{3\eta}$$

Where, U_E = electrophoretic mobility ($V \cdot s \cdot m^{-2}$), ξ = zeta potential (V), ε = dielectric constant, η = viscosity ($m^2 \cdot s^{-1}$) and f(κa) = Henry's function with κ being Debye constant (nm^{-1}) and *a* being the size of the particles (nm).[67] Triplicate experiments were conducted, and the average and standard deviation values are shown in Table 1.

In addition, for set I, the effects of total P/Pb ratios on the zeta potentials of the precipitates could be due to the potential adsorption of lead or phosphate ions onto the precipitates. To understand such processes, the particles were collected from 50 mL precipitation solutions (Table 1, set I) using centrifugal filters (Amicon-15, Millipore), and

were rinsed with ultrapure water multiple times to remove the adsorbed ions. Then the slurry was transferred to ultrapure water (pH ~ 7, adjusted using NaOH) using a pipette, and zeta potential values (ξw, Table 1) were measured after sonicating for 30 min. Similarly, for set V, particles were collected from 50 mL precipitation solutions (Table 1, set V) and rinsed with ultrapure water. Then, the particles were dispersed in water with pH adjusted to that of the precipitation solution conditions (i.e, pH = 5.5, 7.0, and 8.5), and the zeta potential values (ξw, Table 1) were measured. There is a caveat that the particles collected after centrifuging and rinsing with water might have altered water chemistry in the near-surface region. However, the phosphate concentration in the near surface region should be still much lower than that in the original suspensions which had a great excess of phosphate.

For set II, to understand the effects of different electrolyte solutions on zeta potentials of the precipitates, particles were collected from 50 mL precipitation solutions (Table 1, set II) using centrifugal filters (Amicon-15, Millipore) and rinsed with ultrapure water multiple times. Then the collected particles were dispersed both in ultrapure water (ξw, Table 1) and the salt solutions (ξs, Table 1, in 3 mM $NaNO_3$, 1.2 mM $Ca(NO_3)_2$, 1.2 mM $Mg(NO_3)_2$ with IS = 4 mM and pH = 7) for zeta potential measurements. A schematic illustration of the three different types of zeta potential measurements of the precipitates conducted in precipitation solutions, ultrapure water (equilibrated with air and with pH adjustment), and salt solutions (ξp, ξw, and ξs, Table 1) is provided as Figure S2 in the Supporting Information.

Phase and Composition Analysis of Particles Formed in Solutions

Based on GWB calculations, the three pure lead phosphate phases (i.e., hydroxylpyromorphite, $Pb_3(PO_4)_2$, and $PbHPO_4$) were supersaturated under all initial solution conditions (Table 1), while some initial solutions (Table 1) were also saturated with other

phases, which are listed in Table 1. Detailed information of the saturation indices with respect to all supersaturated mineral phases can be found in the Supporting Information (Tables S1 – S2). To identify the mineral phases of the precipitates, particles were collected from the precipitation solutions using centrifugal filters (Amicon-15, Millipore) and were transferred to a gold-coated silicon wafer for GIWAXS (beamline 12 ID-B at Advanced Photon Source (APS), Argonne National Laboratory) and Raman spectroscopy measurements. Detailed information on the GIWAXS and Raman spectroscopy measurements is available in the Supporting Information. In the presence of Ca^{2+} and Mg^{2+}, to study the potential structural incorporation and surface enrichment of these ions in the precipitates, chemical composition analysis of the precipitates was conducted with ICP-MS (details in the Supporting Information).

Results and Discussion

Excess PO_4 Addition Stabilized Lead Phosphate Particles

Based on GWB calculations (Table S1), all initial solutions in set I (Table 1) were supersaturated with respect to hydroxylpyromorphite (SI = 12.6 ± 0.1), $Pb_3(PO_4)_2$ (SI = 7.4 ± 0.2), and $PbHPO_4$ (SI = 1.6 ± 0.3). In addition, the initial solutions with $R_{P/Pb}$ = 10 and 1 (R-10 and R-1 in Table 1) were supersaturated with respect to cerussite (SI = 0.3) and hydrocerussite (SI = 1.6), and the initial solutions with $R_{P/Pb}$ = 60, 10 and 1 (Table 1) were supersaturated with respect to lead hydroxide, cerussite and hydrocerussite. However, GIWAXS and Raman measurements (Figure 1) showed that hydroxylpyromorphite, with the highest SI, was the only mineral phase detected under all solution conditions of set I. Under the initial solution conditions, hydroxylpyromorphite which had the highest SI could precipitate out first. After the precipitation of hydroxylpyromorphite, lead ions were consumed and the SI values with respect to other mineral phases should decrease such that the final solution could be no longer

supersaturated with respect to other lead-containing minerals. Therefore, although most of the initial solutions were supersaturated with respect to multiple mineral phases, hydroxylpyromorphite was the only mineral phase detected.

The size evolution of particles formed in solutions with varied total PO_4/Pb molar ratios ($R_{P/Pb}$, set I in Table 1) are shown in Figure 2A. With $R_{P/Pb} \geq 10$ (i.e., $R_{P/Pb}$ = 1000, 100, 60, and 10), the sizes of particles (40 ± 18 nm) remained unchanged within 1 hr. Size measurements were also conducted for a longer time, and no significant size increase was observed up to 12 days (Figure S1). In contrast to results with excess phosphate relative to lead, in a solution with $R_{P/Pb}$ = 1, the sizes of the particles grew rapidly to 806 ± 39 nm in 1 hr (Figure 2A). The initial fast size increase is indicated by the red line in Figure 2A. Later on, the size reaches plateau (Figure 2A), probably due to that DLS can only accurately measure particles < 1 μm.[68] Here large particles (> 10 μm, Figure 3) formed in solution with $R_{P/Pb}$ = 1 as observed by SEM. SEM observations showed that the big particles were large aggregates of small crystals and not big crystals themselves. Therefore, the fast increase in size of particles formed under $R_{P/Pb}$ = 1 (Figure 3A) was due to fast particle aggregation rather than growth. While for the particles collected from solutions with $R_{P/Pb} > 1$ using the same centrifuging and drying procedures, only small particles and no aggregates were observed by SEM. Therefore, that the aggregates observed by SEM were formed in suspensions, not an artifact of centrifuging or drying the samples in preparation for SEM imaging.

Interactions among particles are described by DLVO theory, according to which the total energy barrier (V_T) for particle aggregation is the sum of the electrostatic repulsive energy (V_{EDL}) and van der Waals (V_{VDW}) attractive energy. Whether the particles in suspension are stable or not is determined by the overall balance of attractive and repulsive energy. Since Hamaker constant

for hydroxylpyromorphite was not reported before, V_T for particle aggregation could not be calculated. In general, particles with absolute zeta potential values lower than ~10-20 mV show relatively fast aggregation, and particles with absolute zeta potential values higher than ~20 – 30 mV show good stability.[69–71] Zeta potential measurements showed that in precipitation solutions with $R_{P/Pb}$ = 1000, 100, 60, and 10, the particles were highly negatively charged with zeta potential values of -46.2 ± 2.3, -39.1 ± 2.4, -40.5 ± 2.0, and -37.9 ± 2.0 mV, respectively (ξp, Table 1). Thus, the strong electrostatic repulsive forces among the particles prevented their aggregation in solution. In contrast, for $R_{P/Pb}$ = 1, the particles were only slightly negatively charged (-9.7 ± 2.7 mV), leading to very weak repulsive forces among the particles and thus their fast aggregation.

As hydroxylpyromorphite formed in all precipitation solutions (Figure 1), the varied zeta potentials of the precipitates measured in precipitation solutions (ξp) with varied $R_{P/Pb}$ were thought to be affected by the adsorption of lead and phosphate ions onto the precipitates. To test this hypothesis, the precipitates were collected from solution, rinsed with ultrapure water multiple times to remove the adsorbed lead and phosphate ions, and dispersed in water (equilibrated with air, pH adjusted to 7.0 by adding NaOH) for zeta potential measurements (ξw). For solutions with excess phosphate relative to lead, i.e., $R_{P/Pb}$ = 1000, 100, 60, and 10 (set I in Table 1), the zeta potentials of precipitates measured in water after the rinsing steps (pH = 7.0) were -22.5 ± 4.5, -25.2 ± 5.0, -21.6 ± 4.3, and -13.0 ± 2.6 mV (ξw, Table 1), which were much less negative than the zeta potentials measured in the precipitation solutions with lead and phosphate ions (ξp, Table 1, -46.2 ± 2.3, -39.1 ± 2.4, -40.5 ± 2.0, and -37.9 ± 2.0 mV). In contrast, for the precipitates collected from solutions with $R_{P/Pb}$ = 1, their zeta potential values in water after rinsing were -12.3 ± 2.5 mV (ξw, Table 1), similar to their zeta potential

(ξp, Table 1, -9.7 ± 2.7 mV) measured in the precipitation solution with equal amounts of total lead and phosphate ions. Therefore, it can be concluded that in precipitation solutions with high aqueous P/Pb ratios, the adsorption of excess amounts of phosphate ions onto the precipitates made the lead phosphate particles highly negatively charged (ξp, Table 1), resulting in their enhanced aqueous stability. In a pilot-scale study with new lead pipe-loops treated with orthophosphate ranging from 0.5 to 5.0 mg PO_4/L, Miller found the lowest total lead concentration with 1.0 mg PO_4/L addition and not with the highest phosphate addition (5.0 mg PO_4/L), suggesting higher total lead concentration in water with excess phosphate addition.[47] Our observation here suggested that the stability of lead phosphate particles was enhanced with excess phosphate addition, which might help explain Miller's pilot-scale observations in pipes. However, more future studies with pipe loops are needed to fully understand the effects of phosphate dosage on particulate lead immobilization.

Promoted Lead Phosphate Aggregation in the Presence of Ca^{2+} and Mg^{2+}

Based on GWB calculations (Table S2 in Supporting Information), both initial solutions in the presence of $Ca(NO_3)_2$ and $Mg(NO_3)_2$ were supersaturated with respect to hydroxylpyromorphite (SI = 12.6), $Pb_3(PO_4)_2$ (SI = 7.4), $PbHPO_4$ (SI = 1.6), lead hydroxide (SI = 0.1), and hydrocerussite (SI = 0.2). Besides, the initial solution in the presence of $Ca(NO_3)_2$ was also supersaturated with hydroxyapatite ($Ca_3(PO_4)_5OH$, SI = 7.7) and $Ca_3(PO_4)_2$ (SI = 0.9) (Table 1, set II). Meanwhile, researchers have reported that significant amounts of Ca ions can be incorporated in the hydroxylpyromorphite structure forming a $(Ca, Pb)_3(PO_4)_5OH$ solid solution,[72,73] resulting in significant shifts in diffraction peaks.[72] However, under our experimental conditions, pure hydroxylpyromorphite was the only mineral phase detected by both GIWAXS and Raman measurements (Figure 1), and no significant structural

297 incorporation of cations in the hydroxylpyromorphite precipitates was detected. Consistently,
298 zeta potentials of the particles collected from precipitation solutions in the presence of $NaNO_3$,
299 $Ca(NO_3)_2$, and $Mg(NO_3)_2$ (Table 1, set II) were similar in 4 mM $NaNO_3$ solution (ξw, Table 1,
300 Figure S2), being -25.2 ± 5.0, -29.1 ± 1.7, and -28.1 ± 1.4 mV, respectively.

301 Size evolutions of precipitates formed in the presence of different cations (set II in
302 Table 1, 3 mM Na^+, 1.2 mM Ca^{2+} and Mg^{2+} with the same IS = 4 mM and pH = 7) showed that
303 divalent cations (Ca^{2+} and Mg^{2+}) promoted aggregation (Figure 2B). In the presence of 3 mM
304 $NaNO_3$, the particle sizes remained unchanged (26 ± 10 nm) within 1 hr. In contrast, in the
305 presence of 1.2 mM $Ca(NO_3)_2$ and $Mg(NO_3)_2$, the particles grew to 649 ± 26 and 565 ± 24 nm
306 within 1 hr. Indicated by the red lines in Figure 2B, fast initial aggregation occurred in 1.2 mM
307 $Ca(NO_3)_2$ and $Mg(NO_3)_2$, similar to $R_{P/Pb}$ = 1 solution. SEM observations (Figures 3B and 3C)
308 also showed the formation of large aggregates.

309 Fast aggregation of the precipitates in the presence of divalent cations can be explained
310 by electrostatic interactions. Particles in the precipitation solutions containing Ca^{2+} and Mg^{2+}
311 were only slightly negatively charged, being -12.6 ± 0.6 and -13.3 ± 0.6 mV (ξp, Table 1),
312 which were much less negatively charged than those formed in the presence of Na^+ (ξp = -39.1
313 ± 2.4 mV). Therefore, only weak electrostatic repulsive forces existed among particles formed
314 in the presence of Ca^{2+} and Mg^{2+}, resulting in their fast aggregation.

315 The mechanisms controlling zeta potential changes (ξp, Table 1, Figure S2) of particles
316 in the precipitation solutions in the presence of Ca^{2+} and Mg^{2+} ions were further explored. The
317 presence of Ca^{2+} and Mg^{2+} ions has been reported to change zeta potentials of various particles
318 (e.g., iron oxide, fullerene, citrate and polyvinylpyrrolidone coated silver particles) by
319 adsorption onto the particle surfaces.[74–76] To test potential surface adsorption of Ca^{2+} and Mg^{2+}

onto the precipitates, lead phosphate particles were collected from the precipitation solutions (set II, Table 1) and rinsed with ultrapure water. Then, zeta potentials of the collected particles were measured in both ultrapure water (ξw, Figure S2) and in the same salt solutions (ξs, Figure S2, 3 mM $NaNO_3$, 1.2 mM $Ca(NO_3)_2$, and 1.2 mM $Mg(NO_3)_2$) of their formation conditions (Table 1, but without lead or phosphate ions). Surprisingly, zeta potential values of these particles in all salt solutions were similar (ξs, Table 1, being -12.1 ± 1.5, -5.7 ± 0.5, and -5.7 ± 0.9 mV in 3 mM $NaNO_3$, 1.2 mM $Ca(NO_3)_2$, and 1.2 mM $Mg(NO_3)_2$ solutions, respectively), and were all similarly less negatively charged than their zeta potentials measured in ultrapure water (ξw, Table 1, -25.2 ± 5.0, -29.1 ± 1.7, and -28.1 ± 1.4 mV, respectively). Such measurements suggested that all cations (Na^+/Ca^{2+}/Mg^{2+}) adsorbed onto these particles and provided similar extents of charge neutralization.

However, significant differences in zeta potentials of the particles were measured in the precipitation solutions with the remaining lead and phosphate ions (ξp, Table 1, Figure S2), being -39.1 ± 2.4, -12.6 ± 0.6, and -13.3 ± 0.6 mV in 3 mM $NaNO_3$, 1.2 mM $Ca(NO_3)_2$, and 1.2 mM $Mg(NO_3)_2$, respectively. Therefore, the presence of lead or phosphate ions must have influenced the adsorption of the cations (Na^+, Ca^{2+}, and Mg^{2+}) onto the precipitates. Xie et al. reported that the presence of phosphate can promote the adsorption of divalent ion (Pb^{2+}) onto iron oxide particles.[77] Here in the precipitation solution containing $NaNO_3$, the precipitates were highly negatively charged due to the adsorption of phosphate; in contrast, the precipitates were much less negatively charged in the presence of $Ca(NO_3)_2$ and $Mg(NO_3)_2$, implying that the presence of phosphate promoted divalent ion (Ca^{2+} and Mg^{2+}) adsorption onto the lead phosphate particles, which neutralized the negative zeta potentials of the particles. The Ca^{2+} and Mg^{2+} enrichment on the precipitate surfaces was further confirmed by the chemical

composition analysis of the precipitates with ICP-MS, as both Ca/Pb or Mg/Pb ratios in surface layers of the precipitates were higher than those in the inner layers. The detailed information about ICP-MS analysis (Table S4) can be found in the Supporting Information.

Lead phosphate aggregation in solutions with varied concentrations of $Ca(NO_3)_2$ or $Mg(NO_3)_2$ (Table S3 in the Supporting Information), typical in water supply systems, was also investigated. Significant aggregation of lead phosphate particles was observed in 1 hr with $Ca(NO_3)_2$ or $Mg(NO_3)_2$ concentrations higher than 0.1 mM, and faster aggregation occurred with higher salt concentrations (Figure S3). The observed aggregation trend could also be explained by zeta potentials .With higher divalent cation concentrations (i.e., 0.5 and 0.8 mM), the particles were much less negatively charged (Table S3, ξp), which resulted in less repulsive forces and faster aggregation.

In sum, divalent cations became enriched in the surfaces of lead phosphate particles to neutralize their initially more negative surface charges that were caused by phosphate adsorption and thereby promote their aggregation. The charge neutralization effect is dependent on the concentrations of cations present in solution, and significant aggregation of lead phosphate particles can occur in 1 hr with only 0.5 mM $Ca(NO_3)_2$ or $Mg(NO_3)_2$.

Structural Incorporation of Anions in Lead Phosphate Particles

Based on GWB calculations (set II, Table S2), all initial solutions containing NaCl, NaF, and $NaHCO_3$ were supersaturated with respect to hydroxylpyromorphite (SI = 12.6 ± 0.1), $Pb_3(PO_4)_2$ (SI = 7.3 ± 0.1), $PbHPO_4$ (SI = 1.6 ± 0.1), and hydrocerussite. The initial solutions were also supersaturated with respect to chloropyromorphite ($Pb_5(PO_4)_3Cl$, CPM in Table 1, SI = 24.9), fluoropyromorphite ($Pb_5(PO_4)_3F$, FPM in Table 1, SI = 12.3), lead hydroxide (SI =

0.1), and cerussite (SI = 1.2), respectively (Table 1, set II). In an *in situ* AFM study of the coupled cerussite dissolution and lead phosphate precipitation, Wang et al. found that the anions Cl^- and F^- substituted for the OH^- group in the lead phosphate precipitates, which affected the phase, size, and shape of the precipitates.[78] Based on GIWAXS and Raman measurements (Figure 1), the only mineral phases detected were the pyromorphite-group minerals.

In solutions with different anions (NO_3^-, Cl^-, HCO_3^-, F^-, set II in Table 1, Figure S4), sizes of lead phosphate particles were similar (40 ± 18 nm) with no significant aggregation observed up to 12 days (Figure S1). Zeta potentials of particles formed in all precipitation solutions (set II, ξp, Table 1) were similar and strongly negatively charged, being -39.1 ± 2.4, -30.7 ± 6.1, -32.3 ± 1.1, and -32.5 ± 1.8 mV in the presence of $NaNO_3$, NaCl, $NaHCO_3$, and NaF, respectively, so the strong electrostatic repulsive forces among the particles resulted in their long-term stability. Although fluoropyromorphite and chloropyromorphite formed in the presence of NaF and NaCl, the structural incorporation of varied channel anions in lead phosphate particles did not affect their zeta potentials, resulting in similar aggregation behaviors. Ion substitution in hydroxylpyromorphite has been reported, e.g. Ca-substituted pyromorphites.[72] Such ion substitution could alter the solubility of lead phosphate precipitates, which could be an interesting future direction.

Retarded Lead Phosphate Aggregation in the Presence of Natural Organic Matter

Previous studies have reported that NOM could adsorb onto various particles (e.g., iron oxide and zinc oxide) and inhibit their aggregation.[79–81] With high lead concentration (0.5 mM) relevant to the lead-contaminated soil environment, Lang et al. reported that the presence of NOM decreased the sizes of the chloropyromorphite precipitates, leading to their enhanced

388 mobility in gravel- and sand-packed columns.[82] To investigate the potential inhibitory effects
389 of NOM on lead phosphate aggregation, experiments with NOM were conducted in a 1.2 mM
390 $CaCl_2$ solution, as fast aggregation of lead phosphate was observed in 1.2 mM $CaCl_2$ without
391 NOM (Figure 2C).

392 With the addition of small amounts of fulvic (0.1 mg C/L) and humic acid (0.05 and 0.1
393 mg C/L), fast aggregation of lead phosphate particles occurred, similar to that in the absence of
394 NOM. However, with the addition of larger amounts of fulvic (0.5, 2, and 5 mg C/L) and
395 humic acid (0.5 and 5 mg C/L), the sizes of lead phosphate particles remained constant during
396 the 1 hr measurements.

397

398 To explain the observed aggregation behaviors, zeta potentials of lead phosphate
399 particles in a $CaCl_2$ precipitation solution were compared in the presence and absence of NOM
400 (set III, Table 1). In the presence of 0, 0.1, 0.5, 2, 5 mg C/L fulvic acid, the zeta potentials (ξp,
401 Table 1) of lead phosphate particles in the precipitation solutions were -13.4 ± 0.5, -14.4 ± 1.7,
402 -16.6 ± 0.7, -18.0 ± 0.5, and -19.3 ± 1.0 mV, respectively. In the presence of 0, 0.05, 0.1, 0.5,
403 and 5 mg C/L humic acid, the zeta potentials (ξp, Table 1) of lead phosphate particles in the
404 precipitation solutions were -13.4 ± 0.5, -15.6 ± 1.3, -15.9 ± 0.9, -16.4 ± 0.6 and -18.3 ± 0.4
405 mV, respectively. The lead phosphate particles were slightly more negatively charged in the
406 $CaCl_2$ precipitation solution in the presence of NOM, resulting in stronger electrostatic
407 repulsion forces among particles and thus slower aggregation. In previous studies, the presence
408 of NOM has been reported to result in more negative zeta potentials of iron oxide particles at
409 neutral pH conditions (pH 7.2), due to the adsorption of deprotonated NOM onto the
410 particles.[49] Previous studies of iron oxide aggregation also suggested the increased steric

411 repulsive forces among particles in the presence of NOM.[80,83,84] Here steric repulsion among
412 lead phosphate particles due to NOM adsorption could have also contributed significantly to
413 the inhibitory effects of NOM on aggregation, especially considering the small changes in zeta
414 potentials of particles in the presence and absence of NOM.

415 ***Promoted Lead Phosphate Aggregation under High Ionic Strength***

416 Size evolution of lead phosphate particles in solutions with different ionic strength
417 values (IS, set IV in Table 1) is shown in Figure 2D. During the 1-hr measurements, under high
418 IS (i.e., 30, 50, 80 and 99 mM), the lead phosphate particles grew rapidly from 40 ± 18 nm to
419 74 ± 10, 414 ± 22, 515 ± 17, and 689 ± 18 nm. In contrast, the particle sizes (40 ± 18 nm) were
420 relatively constant under low IS (i.e., 0.58, 4, 11 and 21 mM) in 1 hr. For long-term size
421 measurements in solutions with low IS, no aggregation occurred for 12 days in solutions with
422 IS = 0.58, 4, and 11 mM. However, the lead phosphate particles under IS = 21 mM started to
423 aggregate after 3 days, with sizes increasing to 168 ± 20 nm (Figure S1 in the Supporting
424 Information).

425 The promotion of aggregation at higher IS could be explained well by the electrostatic
426 interactions among particles according to DLVO theory.[85] The electrostatic repulsion energy
427 (V_{EDL}) among particles could be affected by both the zeta potentials of the particles (ξ) and the
428 Debye length (κ^{-1}). The zeta potential values of particles in precipitation solutions with varied
429 IS (0.58, 4, 11, 21, 30, 50 ,80, and 99 mM) were similar, being -43.7 ± 1.5, -39.1 ± 2.4, -40.1 ±
430 1.3, -34.8 ± 1.2, -38.2 ± 1.6, -37.7 ± 3.4, -38.9 ± 1.0, and -37.3 ± 2.2 mV (ξp, Table 1),
431 respectively. Under higher IS, the electrical double layers among particles were compressed,
432 leading to smaller Debye length, which could result in decreased electrostatic repulsion energy
433 (V_{EDL}) among particles, thus promoting their aggregation.

As required by EPA, total dissolved solids in drinking water should be lower than 500 mg/L.[86] Thus, the IS values in the drinking water supply system are typically below 10 mM. Based on our results, aggregation of lead phosphate particles in a drinking water supply system with IS < 10 mM would not occur within 12 days, because the excess phosphate (as $R_{P/Pb}$ = 100 in set IV) would stabilize the particles. The formation of small lead phosphate particles with long-term stability in suspension may explain the reported high total lead concentrations in tap water after phosphate addition for months at D.C. and Flint, as well as in the pilot-scale pipe-loop studies.[43,44,46,47]

Lead Phosphate Particles with High Stability under pH 5.5-8.5

GWB calculation (Table S2) showed that under pH 8.5, the solution was saturated with respect to lead hydroxide (SI = 1.4), cerussite (SI = 1.2) and hydrocerussite (SI = 4.4). However, both Raman and GIWAXS measurements only detected the formation of hydroxylpyromorphite under all pH conditions (Figure 1).

Figure S5 presents size evolution of particles precipitated under three different pH conditions (5.5, 7.0 and 8.5). Within 1 hr, the particle sizes remained constant, being 65 ± 22, 40 ± 18, and 62 ± 26 nm at pH = 5.5, 7.0, and 8.5, respectively. This is because the particles that formed in the precipitation solutions (set V in Table 1) were all highly negatively charged, with zeta potentials (ξp, Table 1) of -38.7 ± 1.0, -39.1 ± 2.4 and -27.3 ± 3.4 mV at pH 5.5, 7.0, and 8.5, respectively. This explains why particulate lead could remain in high levels in tap water. More detailed discussion of the pH effects on zeta potentials and mineral formation is available in the Supporting Information.

Environmental Implications

Lead release from pipes and fittings in supply systems is a serious threat to public health. Due to low solubility of lead phosphate, phosphate addition has been widely used to reduce lead concentrations in tap water. However, the total lead concentrations in tap water for several water systems have been observed to remain high for several months after phosphate addition. It is possible that dissolved lead concentrations decrease rapidly as lead phosphate forms but that elevated total lead concentrations persist because of the stability of lead phosphates as particles in suspension. In pilot-scale pipe studies, the lowest total lead concentration in water was not achieved with the highest amount of phosphate addition.[47] These previous observations suggested the important roles of particulate lead transport in pipes that are now supported by observations from the current study.

Particulate lead transport is controlled by deposition, which can be affected by aggregation. Here, lead phosphate formation and aggregation were studied under varied aqueous conditions typical in water supply systems. Aggregation of lead phosphate particles was found to be mainly controlled by zeta potentials, which can be affected by the adsorption of excess phosphate ions, divalent cations, and NOM, and not affected much by the presence of anions, the pH conditions investigated here (5.5-8.5), and the ionic strength typical in drinking water systems. pH probably has an effect on aggregation of lead phosphate particles but the effect would not be manifested over the range of pH values for drinking water systems. In addition, enhanced steric repulsive forces by NOM also played a crucial role. Although the addition of excess amounts of phosphate can promote the formation of lead phosphate particles and lower dissolved lead concentration, it could increase the stability of lead phosphate particles, resulting in high particulate lead concentration in tap water. Thus, it is vital to

478 determine an optimal phosphate dosage for lead immobilization in lead pipes. Furthermore,
479 overdosed phosphate can cause eutrophication problems if the phosphate is not adequately
480 removed from the water before it is discharged back to the environment.[87] The presence of
481 Ca^{2+} and Mg^{2+} at concentrations of 0.5 mM or higher promoted the aggregation of lead
482 phosphate particles within 1 hr, which are at levels that are below the 500 mg/L total dissolved
483 solids concentration required for drinking water.[86] In the US, the divalent cation concentrations
484 in drinking water range from very low concentrations to nearly 5 mM for calcium and 2 mM
485 for magnesium.[88,89] For sites with Ca and Mg concentrations larger than 0.5 mM, fast
486 aggregation of lead phosphate particles is expected, suggesting effective total lead removal
487 through phosphate addition. Our findings also suggest that while considering hardness control,
488 it would be beneficial to have some amounts of divalent cations in drinking water distributed
489 through lead pipes, to promote particulate lead removal after phosphate addition. The
490 concentrations of NOM were found to correlate with their retardation effects on lead phosphate
491 aggregation. Therefore, when considering the effects of NOM on drinking water quality, issues
492 of the stability of lead phosphate stability in addition to the formation of disinfection
493 byproducts should be considered.

494 This study focused on systems for which Pb(II) minerals, either carbonates or phosphates,
495 would be the dominant constituents of lead-containing scales and suspended particles. Studying
496 effects of disinfectants which might change the oxidation state of lead-containing particles could
497 be an interesting future direction. This study provides fundamental nanoscale understanding of
498 lead phosphate aggregation, bench-scale and pilot-scale pipe loop studies are needed to verify
499 the effects of aggregation on deposition of particulate lead onto pipe walls.

Acknowledgements

This work was supported by the National Science Foundation (NSF, Awards # 1604042 and #1603717). We thank Dr. Xiaobing Zuo for helping with GIWAXS measurements at beamline 12-ID-B, Advanced Photon Source (APS), Argonne National Laboratory. Use of the facilities at beamline Sector 12 ID-B at APS was supported by the US Department of Energy, Office of Science, Office of Basic Energy Science, under Contract No. DE-AC02- 06CH11357.

Supporting Information Available

Supporting Information includes the details of NOM stock solution preparation and total organic carbon (TOC) measurements, scanning electron microscopy (SEM) measurements, grazing-incidence wide-angle X-ray Scattering (GIWAXS) and Raman spectroscopic measurements for phase identification, enrichment of Ca^{2+} or Mg^{2+} on particle surfaces, comparison of HA/FA effects on aggregation, and effects of pH on the zeta potential and aggregation of particles. This material is available free of charge via the Internet at http://pubs.acs.org.

References

(1) Centers for Disease Control and Prevention. Guidelines for the identification and management of lead exposure in pregnant and lactating women. Available online: https://www.cdc.gov/nceh/lead/publications/leadandpregnancy2010.pdf (accessed on 21 July 2018).

(2) Centers for Disease Control and Prevention. Low level lead exposure harms children: A renewed call for primary prevention. Available online: https://www.cdc.gov/nceh/lead/acclpp/final_document_030712.pdf (accessed on 21 July 2018).

(3) U.S. Environmental Protection Agency. Prohibition on use of lead pipes, solder and flux. Available online: https://www.gpo.gov/fdsys/pkg/CFR-1999-title40-vol15/xml/CFR-1999-title40-vol15-sec141-43.xml (accessed on 24 February 2016).

(4) Lytle, D. A.; Schock, M. R. Formation of Pb(IV) oxides in chlorinated water. *J. Am. Water Work. Assn.* **2005**, *97*, 102–114.

(5) Kim, E. J.; Herrera, J. E. Characteristics of lead corrosion scales formed during drinking water distribution and their potential influence on the release of lead and other contaminants. *Environ. Sci. Technol.* **2010**, *44* (16), 6054–6061.

(6) Triantafyllidou, S.; Schock, M. R.; DeSantis, M. K.; White, C. Low contribution of PbO_2 -coated lead service lines to water lead contamination at the tap. *Environ. Sci. Technol.* **2015**, *49* (6), 3746–3754.

(7) Ng, D.-Q.; Strathmann, T. J.; Lin, Y.-P. Role of orthophosphate as a corrosion inhibitor in chloraminated solutions containing tetravalent lead corrosion product PbO_2. *Environ. Sci. Technol.* **2012**, *46* (20), 11062–11069.

(8) Clark, B. N.; Masters, S. V.; Edwards, M. A. Lead release to drinking water from galvanized steel pipe coatings. *Environ. Eng. Sci.* **2015**, *32* (8), 713–721.

(9) Cantor, A. F. Diagnosing corrosion problems through differentiation of metal fractions. *J. Am. Water Works Assoc.* **2006**, *98* (1), 117–126.

(10) Ng, D.-Q.; Lin, Y.-P. Evaluation of lead release in a simulated lead-free premise plumbing system using a sequential sampling approach. *Int. J. Environ. Res. Public Health* **2016**, *13* (3), 266.

(11) U.S. Environmental Protection Agency. Maximum contaminant level goals and national primary drinking water regulations for lead and copper. Available online: http://www.epa.gov/dwreginfo/lead-and-copper-rule (accessed on 18 September 2018).

(12) Del Toral, M. A.; Porter, A.; Schock, M. R. Detection and evaluation of elevated lead release from service lines: A field study. *Environ. Sci. Technol.* **2013**, *47* (16), 9300–9307.

(13) Patrick, L. Lead toxicity, a review of the literature. Part 1: Exposure, evaluation, and treatment. *Altern. Med. Rev.* **2006**, *11* (1), 2–22.

(14) Olson, E.; Fedinick, K. P. *What's in your water? Flint and beyond*; 2016.

(15) Kim, E. J.; Herrera, J. E.; Huggins, D.; Braam, J.; Koshowski, S. Effect of pH on the concentrations of lead and trace contaminants in drinking water: A combined batch, pipe loop and sentinel home study. *Water Res.* **2011**, *45* (9), 2763–2774.

(16) Cantor, A. F.; Park, J. K.; Vaiyavatjamai, P. Effect of cholorine on corrosion in drinking water systems. *J. Am. Water Work. Assn.* **2003**, *95*, 112–123.

(17) Trueman, B. F.; Gagnon, G. A. A new analytical approach to understanding nanoscale lead-iron interactions in drinking water distribution systems. *J. Hazard. Mater.* **2016**, *311*,

151–157.
(18) Korshin, G. V.; Ferguson, J. F.; Lancaster, A. N. Influence of natural organic matter on the morphology of corroding lead surfaces and behavior of lead-containing particles. *Water Res.* **2005**, *39* (5), 811–818.
(19) Trueman, B. F.; Gagnon, G. A. Understanding the Role of Particulate Iron in Lead Release to Drinking Water. *Environ. Sci. Technol.* **2016**, *50* (17), 9053–9060.
(20) Trueman, B. F.; Sweet, G. A.; Harding, M. D.; Estabrook, H.; Bishop, D. P.; Gagnon, G. A. Galvanic Corrosion of Lead by Iron (Oxyhydr)Oxides: Potential Impacts on Drinking Water Quality. *Environ. Sci. Technol.* **2017**, *51* (12), 6812–6820.
(21) Letterman, R. D.; American Water Works Association. *Water quality and treatment : a handbook of community water supplies*; McGraw-Hill, 1999.
(22) Wang, Y.; Jing, H.; Mehta, V.; Welter, G. J.; Giammar, D. E. Impact of galvanic corrosion on lead release from aged lead service lines. *Water Res.* **2012**, *46* (16), 5049–5060.
(23) Xie, Y.; Wang, Y.; Giammar, D. E. Impact of chlorine disinfectants on dissolution of the lead corrosion product PbO₂. *Environ. Sci. Technol.* **2010**, *44* (18), 7082–7088.
(24) Xie, Y.; Wang, Y.; Singhal, V.; Giammar, D. E. Effects of pH and carbonate concentration on dissolution rates of the lead corrosion product PbO_2. *Environ. Sci. Technol.* **2010**, *44* (3), 1093–1099.
(25) Boyd, G. R.; Dewis, K. M.; Korshin, G. V.; Reiber, S. H.; Schock, M. R.; Sandvig, A. M.; Giani, R. Effects of changing disinfectants on lead and copper release. *J. Am. Water Work. Assn.* **2008**, *100*, 75–87.
(26) Vasquez, F. A.; Heaviside, R.; Tang, Z. (Jason); Taylor, J. S. Effect of free chlorine and chloramines on lead release in a distribution system. *J. Am. Water Work. Assn.* **2006**, *98*, 144–154.
(27) Liu, H.; Korshin, G. V.; Ferguson, J. F. Interactions of Pb(II)/Pb(IV) solid phases with chlorine and their effects on lead release. *Environ. Sci. Technol.* **2009**, *43* (9), 3278–3284.
(28) Edwards, M.; Dudi, A. role of chlorine and chloramine in corrosion of lead-bearing plumbing materials. *J. Am. Water Work. Assn.* **2004**, *96*, 69–81.
(29) Pieper, K. J.; Martin, R.; Tang, M.; Walters, L.; Parks, J.; Roy, S.; Devine, C.; Edwards, M. A. Evaluating water lead levels during the Flint water crisis. *Environ. Sci. Technol.* **2018**, *52* (15), 8124–8132.
(30) Pieper, K. J.; Tang, M.; Edwards, M. A. Flint water crisis caused by interrupted corrosion control: investigating “ground zero” home. *Environ. Sci. Technol.* **2017**, *51* (4), 2007–2014.
(31) Ma, Q. Y.; Logan, T. J.; Traina, S. J. Lead Immobilization from Aqueous Solutions and Contaminated Soils Using Phosphate Rocks. *Environ. Sci. Technol.* **1995**, *29* (4), 1118–1126.
(32) Xu, Y.; Schwartz, F. W. Lead immobilization by hydroxyapatite in aqueous solutions. *J. Contam. Hydrol.* **1994**, *15* (3), 187–206.
(33) Pinto, J. A.; McAnally, A. S.; Flora, J. R. V. Evaluation of lead and copper corrosion control techniques. *J. Environ. Sci. Heal. . Part A Environ. Sci. Eng. Toxicol.* **1997**, *32* (1), 31–53.
(34) US Environmental Protection Agency. *Optimal Corrosion Control Treatment Evaluation Technical Recommendations for Primacy Agencies and Public Water Systems*.
(35) Xie, Y.; Giammar, D. E. Effects of flow and water chemistry on lead release rates from

pipe scales. *Water Res.* **2011**, *45* (19), 6525–6534.
(36) Noel, J. D.; Wang, Y.; Giammar, D. E. Effect of water chemistry on the dissolution rate of the lead corrosion product hydrocerussite. *Water Res.* **2014**, *54*, 237–246.
(37) Chen, C.-S.; Shih, Y.-J.; Huang, Y.-H. Remediation of lead (Pb(II)) wastewater through recovery of lead carbonate in a fluidized-bed homogeneous crystallization (FBHC) system. *Chem. Eng. J.* **2015**, *279*, 120–128.
(38) Edwards, M.; Mcneill, L. S. Effect of phosphate inhibitors on lead release from pipes. *Journal (American Water Works Association)*. American Water Works Association 2002, pp 79–90.
(39) Cao, X.; Ma, L. Q.; Chen, M. ; Hardison, D. W.; Harris, W. G. Weathering of lead bullets and their environment effects at outdoor shooting ranges. *J. Environ. Qual.* **2003**, *32* (2), 526–534.
(40) Keleş, E.; Özer, A. K.; Yörük, S. Removal of Pb^{2+} from aqueous solutions by rock phosphate (low-grade). *Desalination* **2010**, *253* (1–3), 124–128.
(41) Controlling lead in drinking water; Water Research Foundation: Denver, CO, 2015; http://www.waterrf.org/PublicReportLibrary/4409.pdf.
(42) Giammar, D. E.; Xie, L.; Pasteris, J. D. Immobilization of lead with nanocrystalline carbonated apatite present in fish bone. *Environ. Eng. Sci.* **2008**, *25* (5), 725–736.
(43) Churchill, D. M.; Mavinic, D. S.; Neden, D. G.; MacQuarrie, D. M. The effect of zinc orthophosphate and pH-alkalinity adjustment on metal levels leached into drinking water. *Can. J. Civ. Eng.* **2000**, *27* (1), 33–43.
(44) National Service Center for Environmental Publications (NSCEP). *Review of the interim optimal corrosion control treatment for Washington, D.C.*; 2007.
(45) Welter, G.; Schock, M.; Miller, S.; Razza, R.; Giammar, D. *Pipe loop studies of orthophosphate addition for control of lead release in high pH, low DIC waters*; 2015.
(46) Flint residential testing report - results collected through July 5, 2016; State of Michigan: Lansing,MI,2016;https://www.michigan.gov/documents/flintwater/Test_Results_Flint_Sorted_by_Lead_Concentration_513930_7.pdf.
(47) Stephanie A. Miller. Investigation of lead solubility and orthophosphate addition in high pH low DIC water, University of Cincinnati, 2014.
(48) McNeill, L. S.; Edwards, M. Importance of Pb and Cu Particulate Species for Corrosion Control. *J. Environ. Eng.* **2004**, *130* (2), 136–144.
(49) Hu, J.-D.; Zevi, Y.; Kou, X.-M.; Xiao, J.; Wang, X.-J.; Jin, Y. Effect of dissolved organic matter on the stability of magnetite nanoparticles under different pH and ionic strength conditions. *Sci. Total Environ.* **2010**, *408* (16), 3477–3489.
(50) Vikesland, P. J.; Rebodos, R. L.; Bottero, J. Y.; Rose, J.; Masion, A. Aggregation and sedimentation of magnetite nanoparticle clusters. *Environ. Sci. Nano* **2016**, *3* (3), 567–577.
(51) Liu, J.; Dai, C.; Hu, Y. Aqueous aggregation behavior of citric acid coated magnetite nanoparticles: Effects of pH, cations, anions, and humic acid. *Environ. Res.* **2018**, *161*, 49–60.
(52) Korshin, G. V; Ferguson, J. F.; Lancaster, A. N. Influence of natural organic matter on the corrosion of leaded brass in potable water. *Corros. Sci.* **2000**, *42* (1), 53–66.
(53) Broo, A. E.; Berghult, B.; Hedberg, T. Copper corrosion in water distribution systems—the influence of natural organic matter (nom) on the solubility of copper corrosion products. *Corros. Sci.* **1998**, *40* (9), 1479–1489.
(54) Stankus, D. P.; Lohse, S. E.; Hutchison, J. E.; Nason, J. A. Interactions between natural

organic matter and gold nanoparticles stabilized with different organic capping agents. *Environ. Sci. Technol.* **2011**, *45* (8), 3238–3244.
(55) Peng, J. Geochemical conditions and design considerations affecting electrode-induced removal of uranium(VI) and technetium(VII) from acidic groundwater, Carnegie Mellon University, 2012.
(56) Schock, M. R.; Lytle, D. A.; Sandvig, A. M.; Clement, J.; Harmon, S. M. Replacing polyphosphate with silicate to solve lead, copper, and source water iron problems. *J. Am. Water Works Assoc.* **2005**, *97*, 84–93.
(57) Davidson, C. M.; Peters, N. J.; Britton, A.; Brady, L.; Gardiner, P. H. E.; Lewis, B. D. Surface analysis and depth profiling of corrosion products formed in lead pipes used to supply low alkalinity drinking water. *Water Sci. Technol.* **2004**, *49* (2), 49–54.
(58) Hopwood, J. D.; Davey, R. J.; Jones, M. O.; Pritchard, R. G.; Cardew, P. T.; Booth, A. Development of chloropyromorphite coatings for lead water pipes. *J. Mater. Chem.* **2002**, *12* (6), 1717–1723.
(59) Zhang, C.; Dai, C.; Zhang, H.; Peng, S.; Wei, X.; Hu, Y. Regeneration of mesoporous silica aerogel for hydrocarbon adsorption and recovery. *Mar. Pollut. Bull.* **2017**, *122* (1–2), 129–138.
(60) Dai, C.; Lin, M.; Hu, Y. Heterogeneous Ni- and Cd-bearing ferrihydrite precipitation and recrystallization on quartz under acidic pH condition. *ACS Earth Sp. Chem.* **2017**, *1* (10), 621–628.
(61) Liu, J.; Wu, X.; Hu, Y.; Dai, C.; Peng, Q.; Liang, D. Effects of Cu(II) on the adsorption behaviors of Cr(III) and Cr(VI) onto kaolin. *J. Chem.* **2016**, 1–11.
(62) Tang, R.; Dai, C.; Li, C.; Liu, W.; Gao, S.; Wang, C. Removal of methylene blue from aqueous solution using agricultural residue walnut shell: Equilibrium, kinetic, and thermodynamic studies. *J. Chem.* **2017**, 1–10.
(63) Dai, C.; Zuo, X.; Cao, B.; Hu, Y. Homogeneous and heterogeneous $(Fe_x, Cr_{1-x})(OH)_3$ precipitation: Implications for Cr sequestration. *Environ. Sci. Technol.* **2016**, *50* (4), 1741–1749.
(64) Dai, C.; Hu, Y. Fe(III) hydroxide nucleation and growth on quartz in the presence of Cu(II), Pb(II), and Cr(III): Metal hydrolysis and adsorption. *Environ. Sci. Technol.* **2015**, *49* (1), 292–300.
(65) Dai, C.; Stack, A. G.; Koishi, A.; Fernandez-Martinez, A.; Lee, S. S.; Hu, Y. Heterogeneous nucleation and growth of barium sulfate at organic–water interfaces: Interplay between surface hydrophobicity and Ba^{2+} adsorption. *Langmuir* **2016**, *32* (21), 5277–5284.
(66) Dai, C.; Liu, J.; Hu, Y. Impurity-bearing ferrihydrite nanoparticle precipitation/deposition on quartz and corundum. *Environ. Sci. Nano* **2018**, *5* (1), 141–149.
(67) Jones, D. J.; Buechi, F.; Lyons, K. S. (Eds.). Polymer Electrolyte Fuel Cells 17 (PEFC 17). Electrochemical Society. 2017
(68) Measurement of particle size distributions https://www.malvernpanalytical.com/en/products/measurement-type/particle-size (accessed Aug 9, 2018).
(69) Honary, S.; Zahir, F. Effect of zeta potential on the properties of nano-drug delivery systems-A review (Part 2). *Trop. J. Pharm. Res.* **2013**, *12* (2), 265–273.
(70) Cho, W.-S.; Thielbeer, F.; Duffin, R.; Johansson, E. M. V.; Megson, I. L.; MacNee, W.; Bradley, M.; Donaldson, K. Surface functionalization affects the zeta potential, coronal

stability and membranolytic activity of polymeric nanoparticles. *Nanotoxicology* **2014**, *8* (2), 202–211.
(71) Chibowski, E.; Szcześ, A. Zeta potential and surface charge of DPPC and DOPC liposomes in the presence of PLC enzyme. *Adsorption* **2016**, *22* (4–6), 755–765.
(72) Hopwood, J. D.; Derrick, G. R.; Brown, D. R.; Newman, C. D.; Haley, J.; Kershaw, R.; Collinge, M. The identification and synthesis of lead apatite minerals formed in lead water pipes. *J. Chem.* **2016**, *2016*, 1–11.
(73) Markl, G.; Marks, M. A. W.; Holzapfel, J.; Wenzel, T. Major, minor, and trace element composition of pyromorphite-group minerals as recorder of supergene weathering processes from the Schwarzwald mining district, SW Germany. *Am. Mineral.* **2014**, *99* (5–6), 1133–1146.
(74) Kretzschmar, R.; Sticher, H. Transport of humic-coated iron oxide colloids in a sandy soil: influence of Ca^{2+} and trace metals. *Environ. Sci. Technol.* **1997**, *31* (12), 3497–3504.
(75) Chen, K. L.; Elimelech, M. Aggregation and deposition kinetics of fullerene (C60) nanoparticles. **2006**.
(76) Huynh, K. A.; Chen, K. L. Aggregation kinetics of citrate and polyvinylpyrrolidone coated silver nanoparticles in monovalent and divalent electrolyte solutions. *Environ. Sci. Technol.* **2011**, *45* (13), 5564–5571.
(77) Barnett, M. O.; Kent, D. B. *Book series: Developments in earth and environmental sciences*; 2007.
(78) Wang, L.; Putnis, C. V.; Ruiz-Agudo, E.; King, H. E.; Putnis, A. Coupled dissolution and precipitation at the cerussite-phosphate solution interface: Implications for immobilization of lead in soils. *Environ. Sci. Technol.* **2013**, *47* (23), 13502–13510.
(79) Cao, X.; Ma, L. Q.; Singh, S. P.; Zhou, Q. Phosphate-induced lead immobilization from different lead minerals in soils under varying pH conditions. *Environ. Pollut.* **2008**, *152* (1), 184–192.
(80) Baalousha, M. Aggregation and disaggregation of iron oxide nanoparticles: Influence of particle concentration, pH and natural organic matter. *Sci. Total Environ.* **2009**, *407* (6), 2093–2101.
(81) Zhou, D.; Keller, A. A. Role of morphology in the aggregation kinetics of ZnO nanoparticles. *Water Res.* **2010**, *44* (9), 2948–2956.
(82) Lang, F.; Kaupenjohann, M. Effect of dissolved organic matter on the precipitation and mobility of the lead compound chloropyromorphite in solution. *Eur. J. Soil Sci.* **2003**, *54* (1), 139–148.
(83) Baalousha, M.; Manciulea, A.; Cumberland, S.; Kendall, K.; Lead, J. R. Aggregation and surface properties of iron oxide nanoparticles: Influence of pH and natural organic matter. *Environ. Toxicol. Chem.* **2008**, *27* (9), 1875.
(84) Diegoli, S.; Manciulea, A. L.; Begum, S.; Jones, I. P.; Lead, J. R.; Preece, J. A. Interaction between manufactured gold nanoparticles and naturally occurring organic macromolecules. *Sci. Total Environ.* **2008**, *402* (1), 51–61.
(85) Li, W.; Liu, D.; Wu, J.; Kim, C.; Fortner, J. D. Aqueous aggregation and surface deposition processes of engineered superparamagnetic iron oxide nanoparticles for environmental applications. *Environ. Sci. Technol.* **2014**, *48* (20), 11892–11900.
(86) US Environmental Protection Agency. *Secondary drinking water standards: guidance for nuisance chemicals*.
(87) Malati, M. A.; Fox, I. A review of the role of bed deposits in the phosphate eutrophication

of lakes and rivers. *Int. J. Environ. Stud.* **1985**, *26* (1–2), 43–54.
(88) Morr, S.; Cuartas, E.; Alwattar, B.; Lane, J. M. How much calcium is in your drinking water? A survey of calcium concentrations in bottled and tap water and their significance for medical treatment and drug administration. *HSS J.* **2006**, *2* (2), 130–135.
(89) Azoulay, A.; Garzon, P.; Eisenberg, M. J. Comparison of the mineral content of tap water and bottled waters. *J. Gen. Intern. Med.* **2001**, *16* (3), 168–175.

Table 1. Initial experimental conditions and zeta potentials of precipitates

	Set	$R_{P/Pb}$	Pb[a], μM	P[a], mM	NO_3^-, mM	Na^+, mM	IS[b], mM	pH[b]	Other saturated mineral phases[c]	ξp[d], mV	ξw[e], mV	ξs[f], mV
I	R-1000	1000:1	1.40	1.40	1.66	3.78	4	7.0	N/A	-46.2 ± 2.3	-22.5 ± 4.5	N/A
	R-100	100:1	3.20	0.32	3.01	3.51	4	7.0	HCR	-39.1 ± 2.4	-25.2 ± 5.0	N/A
	R-60	60:1	3.70	0.222	3.56	3.94	4	7.0	$Pb(OH)_2$, HCR	-40.5 ± 2.0	-21.6 ± 4.3	N/A
	R-10	10:1	6.90	6.90×10^{-2}	3.76	3.92	4	7.0	$Pb(OH)_2$, CRU, HCR	-37.9 ± 2.0	-13.0 ± 2.6	N/A
	R-1	1:1	24.6	2.46×10^{-2}	3.85	3.87	4	6.7	$Pb(OH)_2$, CRU, HCR	-9.7 ± 2.7	-12.3 ± 2.5	N/A
II	1.2 mM $Ca(NO_3)_2$	100:1	3.20	0.32	2410	0.543	4	7.0	$Pb(OH)_2$, HCR, APT, HAP	-12.6 ± 0.6	-29.1 ± 1.7	-5.7 ± 0.5
	1.2 mM $Mg(NO_3)_2$	100:1	3.20	0.32	2410	0.552	4	7.0	$Pb(OH)_2$, HCR	-13.3 ± 0.6	-28.1 ± 1.4	-5.7 ± 0.9
	3.6 mM NaCl	100:1	3.40	0.34	6.80	4.14	4	7.0	HCR, CPM	-30.7 ± 6.1	-31.3 ± 2.6	-12.5 ± 1.7
	3.2 mM NaF	100:1	3.20	0.32	6.40	3.74	4	7.0	$Pb(OH)_2$, HCR, FPM	-32.3 ± 1.1	-26.0 ± 3.7	-11.1 ± 2.9
	3.1 mM $NaHCO_3$	100:1	6.44	0.64	12.9	3.74	4	7.0	CRU, HCR	-32.5 ± 1.8	-29.4 ± 3.3	-18.7 ± 2.6
III	1.2 mM $CaCl_2$	100:1	3.20	0.32	6.40	0.547	4	7.0	$Pb(OH)_2$, HCR, CPM, APT, HAP	-13.4 ± 0.5	N/A	N/A
	$CaCl_2$ + FA	100:1	3.20	0.32	6.40	0.547	4	7.0	$Pb(OH)_2$, HCR, CPM, APT, HAP	-17.1 ± 2.1	N/A	N/A
	$CaCl_2$ + HA	100:1	3.20	0.32	6.40	0.547	4	7.0	$Pb(OH)_2$, HCR, CPM, APT, HAP	-16.6 ± 1.2	N/A	N/A
IV	IS-0.58 – 99	100:1	3.00 – 9.10	0.30 – 0.91	6.00×10^{-3} – 100	0.471 – 101	0.58 – 99	7.0	$Pb(OH)_2$, HCR	-38.7 ± 2.6	N/A	N/A

V	pH-5.5	100:1	36	3.60	7.20×10^{-2}	3.71	4	5.5	N/A	-38.7 ± 1.0	-13.6 ± 1.4	N/A
	pH-8.5	100:1	4.40	0.44	1.01	3.55	4	8.5	$Pb(OH)_2$, CRU, HCR	-27.3 ± 3.4	-14.1 ± 1.4	N/A

Note: Pb[a] and P[a]: calculated total lead and phosphate concentrations, which were consistent with measurements using ICP-MS. IS[b] (Ionic Strength) and pH[b] were calculated using GWB based on initial solution conditions. Conductivity and pH were measured at the beginning and end of the DLS measurements, and no significant differences were observed. Other saturated mineral phases[c]: All solutions were supersaturated with three pure lead phosphate phases (hydroxylpyromorphite, $Pb_3(PO_4)_2$, and $PbHPO_4$). Here, other saturated mineral phases are listed, where HCR, CRU, APT, HAP, CPM, and FPM represent hydrocerussite, cerussite, apatite, hydroxyapatite, chloropyromorphite, and fluoropyromorphite, respectively. Detailed information of the calculated saturation indices (SI) for all minerals can be found in the Supporting Information. ξp[d]: zeta potentials of particles in precipitation solutions. ξw[e]: zeta potentials of particles in water. ξs[f]: zeta potentials of particles in salt solutions as illustrated in Figure S3.

List of Figures

Figure 1. Phase identification of precipitates collected from solutions (Table 1). (A) GIWAXS measurements: Hydroxylpyromorphite was the only mineral phase detected under solution conditions of R-1, 1.2 mM $Ca(NO_3)_2$, 1.2 mM $Mg(NO_3)_2$, 3.1 mM $NaHCO_3$, and pH-8.5. In the presence of 3.6 mM NaCl, it is hard to identify whether the precipitates were hydroxylpyromorphite or chloropyromorphite due to their similar diffraction patterns. In the presence of 3.2 mM NaF, fluoropyromorphite was the only mineral phase detected. (B) Raman spectroscopy of hydroxylpyromorphite standard sample (a), as well as precipitates formed under various conditions (b-g). The precipitates formed under (d) $R_{P/Pb} = 1$, in the presence of (c) 3.1 mM $NaHCO_3$, (e) 1.2 mM $Mg(NO_3)_2$, and (f) 1.2 mM $Ca(NO_3)_2$) were identified to be hydroxylpyromorphite. In the presence of (b) 3.6 mM NaCl and (g) 3.2 mM NaF, the decreased intensity of OH-band (3550-3600 cm^{-1}) indicated various degrees of channel anion (OH^-) substitution by Cl^-/F^- and the potential formation of chloropyromorphite and fluoropyromorphite.

Figure 2. DLS measurements of size evolutions of lead phosphate particles in precipitation solutions (Table 1, sets I - IV) within 1 hr. (A) Set I, $R_{P/Pb}$ = 1000, 100, 60, 10, and 1. (B) Set II, with the addition of 1.2 mM $Ca(NO_3)_2$, 1.2 mM $Mg(NO_3)_2$, or 1.2 mM $CaCl_2$ (C) Set III, in 1.2 mM $CaCl_2$ solutions, with the addition of 0- 5 mg C/L fulvic or humic acid. (D) Set IV, IS = 0.58 mM, 4 mM, 11 mM, 21 mM, 30 mM, 50 mM, 80 mM, and 99 mM. The size data were continuously recorded every 15 s for 1 hr. The sizes of lead phosphate particles were reported by number-based calculation using the refractive index of lead phosphate (2.048). All solutions were saturated with respect to hydroxylpyromorphite with SI = 12.6 at pH ~ 7.

Figure 3. SEM observations of aggregates formed under varied solution conditions: (A) $R_{P/Pb}$ = 1, (B) in the presence of 1.2 mM $Ca(NO_3)_2$, and (C) in the presence of 1.2 mM $Mg(NO_3)_2$.

Figure 1

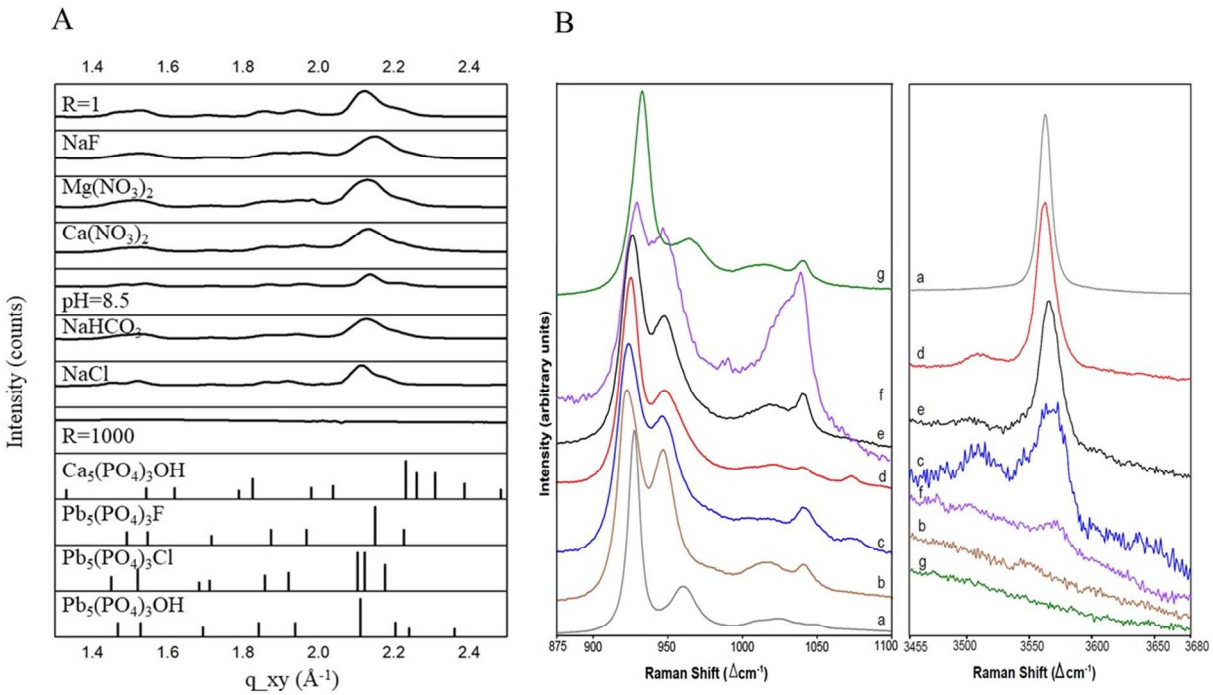
A
B
1.4
1.6
1.8
2.0
2.2
2.4
R=1
NaF
Mg(NO3)2
Ca(NO3)2
pH=8.5
NaHCO3
NaCl
R=1000
Ca5(PO4)3OH
Pb5(PO4)3F
Pb5(PO4)3Cl
Pb5(PO4)3OH
Intensity (counts)
q_xy (Å-1)
Intensity (arbitrary units)
875
900
950
1000
1050
1100
Raman Shift (Δcm-1)
3455
3500
3550
3600
3650
3680
Raman Shift (Δcm-1)
a
b
c
d
e
f
g

Figure 2

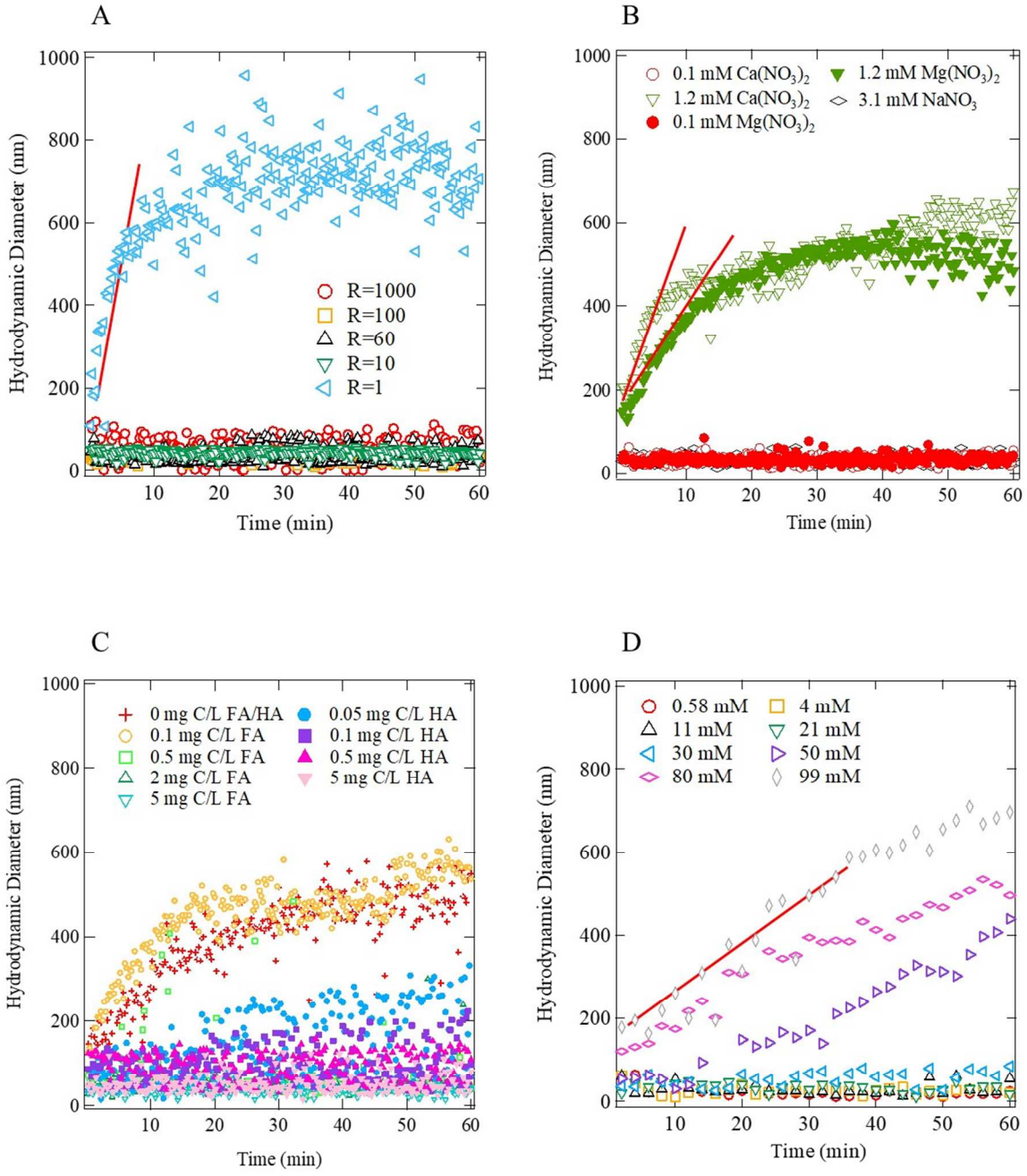
A
Hydrodynamic Diameter (nm)
Time (min)
R=1000
R=100
R=60
R=10
R=1
B
0.1 mM Ca(NO3)2
1.2 mM Ca(NO3)2
0.1 mM Mg(NO3)2
1.2 mM Mg(NO3)2
3.1 mM NaNO3
C
0 mg C/L FA/HA
0.1 mg C/L FA
0.5 mg C/L FA
2 mg C/L FA
5 mg C/L FA
0.05 mg C/L HA
0.1 mg C/L HA
0.5 mg C/L HA
5 mg C/L HA
D
0.58 mM
11 mM
30 mM
80 mM
4 mM
21 mM
50 mM
99 mM

Figure 3

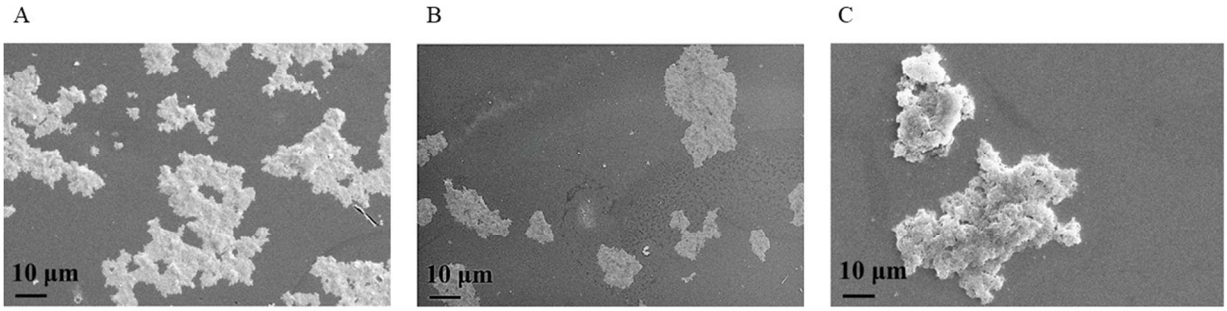

TOC

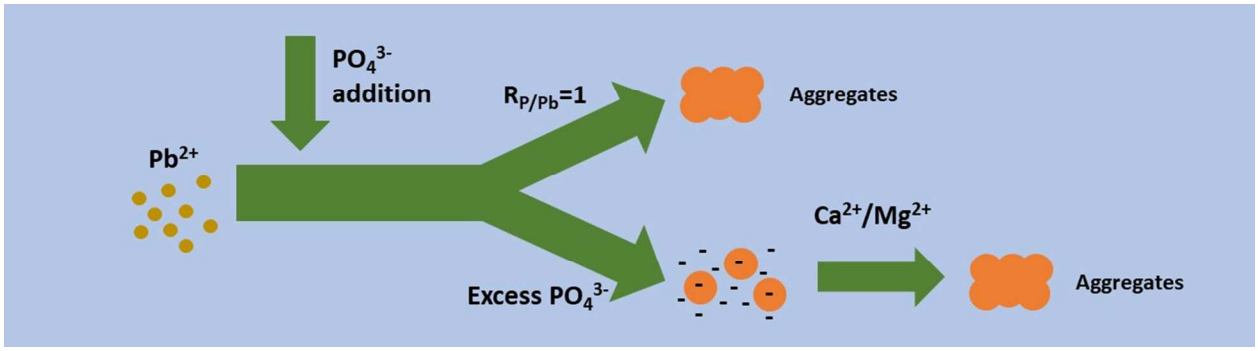
PO_4^{3-} addition
$R_{P/Pb}$=1
Aggregates
Pb^{2+}
Ca^{2+}/Mg^{2+}
Excess PO_4^{3-}
Aggregates